Journal of Biomedical Optics

SPIEDigitalLibrary.org/jbo

Target molecule imaging on tissue specimens by fluorescent metal nanoprobes

Jian Zhang
Yi Fu
Xuehong Xu
Joseph R. Lakowicz

SPIE

Target molecule imaging on tissue specimens by fluorescent metal nanoprobes

Jian Zhang,[a] Yi Fu,[a] Xuehong Xu,[b] and Joseph R. Lakowicz[a]
[a]University of Maryland School of Medicine, Center for Fluorescence Spectroscopy, Department of Biochemistry and Molecular Biology, 725 West Lombard Street, Baltimore, Maryland 21201
[b]University of Maryland School of Medicine, Department of Physiology, Center for Biomedical Engineering Technology, 725 West Lombard Street, Baltimore, Maryland 21201

Abstract. In this paper, fluorescence metal nanoshells (FMNs) were synthesized for target molecule detection on tissue specimens by fluorescence imaging method. FMNs were made with 40 nm silica spherical cores and 10 nm silver shells. $Ru(bpy)_3^{2+}$ complexes were encapsulated in the silica cores for fluorescence properties. Avidin molecules were covalently bound on FMNs and formed avidin-Ag complexes could be site-specially conjugated on bone tissue specimens. Fluorescence intensity and lifetime images were recorded on a time-resolved confocal microscope. Imaging measurements showed that the emissions by avidin-FMN complexes could be distinctly isolated as individuals from the cellular backgrounds on lifetime images even when the tissues were stained with additional organic dyes. This observation demonstrates that the metal nanoprobes can be used for single target molecule detection on tissues during fluorescence imaging measurements. [DOI: 10.1117/1.3644394]

Keywords: fluorescence metal nanoshell; molecular imaging agent; bone tissue specimen; fluorescent cell imaging; time-resolved confocal microscope; single target molecule detection.

Paper 11332RR received Jun. 29, 2011; revised manuscript received Sep. 8, 2011; accepted for publication Sep. 9, 2011; published online Oct. 26, 2011.

1 Introduction

The fluorescence imaging method has been widely used in studying signaling pathways and disease diagnosis.[1,2] Imaging agents can play an important role in labeling target molecules for detecting the amounts and distributions of target molecules in the samples. Presently, most imaging agents are composed of conventional organic fluorophores.[3] However, there are technical shortcomings for organic dyes that can severely limit their applications.[4,5] First, the optical brightness or photon emission rates of most organic dyes are hindered by their intrinsic properties, and thus may lead to difficulty in single probe detection. The detections are found to become more difficult when the emissions from the probes are interfered by cellular autofluorescence. Second, the organic dyes often display rapid photobleaching and/or strong photoblinking, which can reduce the observation time in imaging measurements. Third, with advances of fluorescence lifetime imaging microscopy, lifetime imaging technology is widely used as a powerful tool in the target molecule detections.[6] However, most organic dyes have their lifetimes in a range of 2 to 5 ns, close to the cellular autofluorescence. As a result, the emission signals from the probes cannot be isolated from the cellular backgrounds in lifetime imaging. Hence, there is a basic need to develop novel imaging agents that have improved optical properties on their emission intensity and lifetime.

In the past decade, there has been a rapid development in the understanding of interaction of a fluorophore with a metal nanoparticle.[7–9] Within a near-field range, such an interaction can dramatically alter the optical properties of the fluorophore including increasing the emission intensity and decreasing the lifetime.[10] Additionally, by the near-field interaction, the photobleaching time of the fluorophore can be increased and photoblinking opportunity can be reduced.[11] Based on these observations, the fluorescence metal nanoparticles have been developed as intensity and lifetime imaging agents for detecting the target molecules within the cells. Typically, these metal nanoprobes are designed in two configurations: metal nanospheres with fluorophores immobilized on external layers[12] and metal nanoshells with fluorophores within cores.[13,14] Both configurations were found to display improved optical properties, and their emission signals were observed to be distinctly distinguishable in the cell images.[15,16] We are particularly interested in the metal nanoshells because there are uniform and intensive electric fields throughout core areas,[17–19] and thus the dyes in the cores can be interacted efficiently with metal plasmon resonances, leading to great improvements on their optical properties.

In current biological researches, the metal nanoparticles are mostly made with gold rather than silver because gold has better chemical stability and surface chemistry.[7,8] However, in this research, we prefer silver. First, the silver intends to enhance the emission from the excited dye in near-field interaction but gold tends to quench or weakly enhance the emission. Second, silver nanoshells display a plasmon resonance at 430 nm close to excitation wavelength of Ru(II) complexes that were used as dyes in this research. Thus, there is a good coupling interaction between the dye and silver shell. In contrast, the gold shell is known to display a plasmon resonance at 550 nm or higher,[8] so the coupling interaction is relatively weaker. Our recently unpublished results also showed that the gold shell can interact

Address all correspondence to: Jian Zhang, University of Maryland School of Medicine, 725 West Lombard Street, Baltimore, Maryland 21201; Tel: 410-706-7500; Fax: 410-706-8408; E-mail: jian@cfs.biomet.umaryland.edu.

1083-3668/2011/16(11)/116004/6/$25.00 © 2011 SPIE

with near-infrared dyes and the silver shell can interact well with the dyes in visible range. So far, the metal nanoshell probes have been used as imaging agents for single microRNA detection in lung cancer cells and detection of CXCR4 receptors on T-cells for HIV study.[20,21]

Compared with cell lines, tissue specimens are known to have stronger cellular emission backgrounds from autofluorescence and scattering.[22] Therefore, the single target molecule detection on the tissues becomes more difficult. In this research, the metal nanoshells were used as imaging agents to site-specially conjugate with the target molecules on the tissue specimens for intensity and lifetime imaging. Typically, the metal nanoshell probes were covalently bound with the avidin molecules on the avidin molecules on the external layers. The bone tissues from the tail of a mouse were first biotinylated and then incubated with avidin-fluorescence metal nanoshell (FMN) complexes. Fluorescence intensity and lifetime images of the tissue samples were recorded on a time-resolved confocal microscope. The emission signals from the metal nanoprobes were evaluated at single probe level on the collected images.

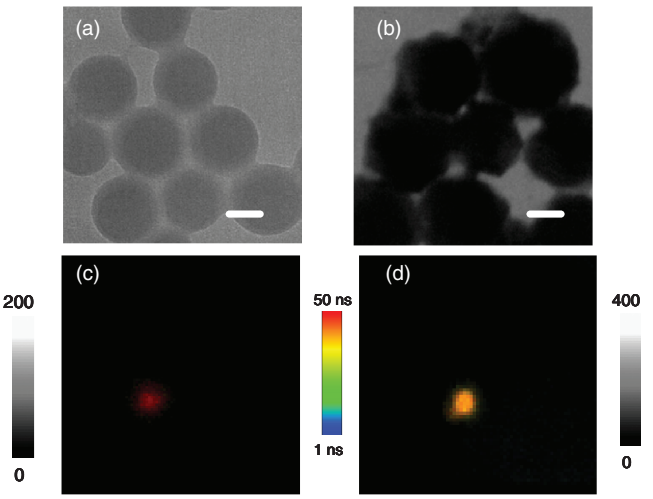

Fig. 1 TEM images and single nanoparticle for (a) and (c) silica spheres and for (b) and (d) silver nanoshells. The scale bars in TEM images are 20 nm. The scales for the fluorescence images are 5×5 μm and the resolutions are 100×100 pixel with an integration of 0.6 ms/pixel.

2 Materials and Methods

All reagents and spectroscopic grade solvents were purchased from Sigma-Aldrich. Cy5-avidin conjugate was purchased from Invitrogen. The dialysis membrane (MWCO 4000) was purchased from Spectrum Laboratories, Inc. Nanopure water (>18.0 MΩ.cm) from a Millipore Milli-Q was used in all experiments. (2-mercapto-propionylamino) acetic acid 2,5-dioxo-pyrrolidin-1-ylester was synthesized as described previously.[23]

2.1 *Preparation of Avidin-Bound FMNs*

The silica spheres and silver shells were made in a strategy as previously described.[19,20] To immobilize the $Ru(bpy)_3^{2+}$ complexes in the silica spheres, the $Ru(bpy)_3^{2+}$ complex (1×10^{-6} M) was co-dissolved with 1.0×10^{-2} M tetraethyl orthosilicate in reaction solution. Formed silica spheres were aminated with 3-aminopropyltrimethoxy silane and then coated with 10 nm silver layers. The metal nanoshells were coated with monolayers of hexa(ethyleneglycol)mono-11-(acetylthio)undecyl ether on surfaces.[24] To bind with avidin molecules, the metal nanoshells were partially substituted by (2-mercapto-propionylamino) acetic acid 2,5-dioxo-pyrrolidin-1-ylester via ligand exchange reaction,[23] and then co-dissolved with excess amount of avidin in 10 mm phosphate buffered saline (PBS) buffer at pH 8.2.[25] The recovered avidin-bound metal nanoshells were dispersed in 10 mm PBS buffer at pH 7.4.

The silica spheres and silver nanoshells were evaluated on transmission electron micrographs (TEM), appearing approximately homogeneous in size distribution and an average diameter of 40 and 60 nm [Figs. 1(a) and 1(b)], respectively. Therefore, the thickness of a metal shell on 40 nm silica cores was estimated to be approximately 10 nm.

2.2 *Tissue Specimens and Conjugation with Avidin-FMN Complexes*

Bone tissue specimens are known to have strong autofluorescence backgrounds in imaging measurements. In this research, the tissue specimens were harvested from the tail of a mouse at postnatal day 26. The tissues were immediately snapped and frozen with liquid nitrogen. Frozen sections were carried out with cryostat at -20°C embedded with optimal cutting temperature (OCT) media, cut at thickness of 5 to 10 μm, and dried in air for 40 min. The tissue specimens were fixed in 4% paraformaldehyde and rinsed with 10 mm PBS buffer at pH 7.4. All animal procedures were conducted under guidelines approved by the University of Maryland, Baltimore School of Medicine Institutional Animal Care and Use Committee. C57BL/6J mice (The Jackson Laboratory; Bar Harbor, Maine) were bred under standard conditions and sacrificed by cervical dislocation.

Tissue specimens were biotinylated with 1 nm EZ-link sulfo-NHS-biotin for 30 min in 10 mm PBS buffer solution at 4°C.[26,27] The tissues were then incubated with 1 nm avidin-FMN complexes at 4°C for 2 h.[16] After washing thoroughly with 10 mm PBS buffer and drying in air, the tissues were used for fluorescence intensity and lifetime tissue imaging measurements.

2.3 *Spectral Measurements, Fluorescence Tissue Imaging, and TEM Measurements*

Absorption spectra were monitored with a Hewlett Packard 8453 spectrophotometer. Ensemble fluorescence spectra were detected on a Cary eclipse fluorescence spectrophotometer. The imaging measurements were performed on a time-resolved scanning confocal microscope (MicroTime 200, PicoQuant).[19,20] Transmission electron micrographs were taken with a side-entry Philips electron microscope at 120 keV. Samples were cast from water solutions onto standard carbon-coated (200 to 300 Å) Formvar films on copper grids (200 mesh) by placing a droplet of diluted aqueous sample solution onto the grid. The size distribution of metal shells was analyzed with Scion Image Beta Release 2 from at least 200 nanoparticles.

3 Results and Discussion

In this case, metal nanoshells were made with 40 nm silica cores and 10 nm silver shells.[13,14] There were approximate 100 $Ru(bpy)_3^{2+}$ complexes incorporated into a single silica core. To improve the chemical stability of FMNs in buffer solution and reduce their nonspecial conjugations with the tissue specimens, we coated FMNs with monolayers of polyethylene glycol (PEG)-like ligands. Through a two-step surface reaction, avidin molecules were covalently bound on FMNs (Refs. 20 and 21) forming avidin-FMN complexes. The avidin-FMN complexes showed a plasmon resonance absorbance centered at 430 nm. Upon excitation at 450 nm, the avidin-FMN complexes displayed an emission maximum at 608 nm. Through a typical NaCN treatment,[28] we estimated that there was an average of 5.6 avidin molecules bound on a single metal nanoshell.

We determined optical properties of single avidin-FMN complexes on a time-resolved confocal microscope [Fig. 1(d)]. As a control, the emission properties of metal-free silica spheres were also detected under the same conditions [Fig. 1(c)]. The samples were excited with a laser line at 470 nm, close to the maximal excitation wavelength of $Ru(bpy)_3^{2+}$ complexes. It was observed that most emission signals from either metal nanoprobes or silica spheres were round images and regarded from single nanoparticles, a result of the nanoparticle concentration being diluted to nanomole in solution prior to being cast on the coverslips. It was furthermore verified by the TEM measurements in which the samples were made under the same conditions on the copper grids [Figs. 1(a) and 1(b)]. To achieve the optical properties from the single nanoparticles, we collected the intensities and lifetimes from at least 50 emission spots and the results are shown in Fig. 2. Due to near-field interactions, the intensity of avidin-FMN complexes was found to increase approximately 6-fold in comparison with the silica spheres [Fig. 2(a)], whereas the lifetime of the avidin-FMN complexes was found to decrease approximately 12-fold [40 ns in Fig. 2(b). The lifetime of the silica spheres was measured to be approximately 600 ns by ensemble time-resolved system in our previous publication[13]]. We also noticed that although the lifetime of metal nanoprobes is shortened, the value is still longer than the lifetime of cellular autofluorescence (2 to 5 ns),[2] which will likely result in distinct isolations of emission signals of metal nanoprobes from the cellular backgrounds in lifetime imaging. On the other hand, the metal nanoprobes have increased emission intensity relative to the silica spheres. Thus, the interference from the cellular autofluorescence is greatly reduced, leading to a significant improvement on the isolations of emission signals in lifetime imaging.

Bone tissue specimens are known to have denser matter structures and thus have stronger cellular backgrounds from autofluorescence and scattering in imaging. In comparison with cell lines or other tissues, the detection of single target molecules by fluorescence imaging method is more difficult on the bone tissues. To circumvent this problem, we used the avidin-FMN complexes as imaging agents to site-specially bind with the bone tissue specimens. Typically, the bone tissues were first biotinylated with EZ-link sulfo-NHS-biotin[25,26] and then incubated with the avidin-FMN complexes via biotin-avidin interactions.[21] Fluorescence intensity and lifetime images of conjugated tissue samples were recorded on the time-resolved confocal microscope and the images are presented in Fig. 3. It is shown that the avidin-FMN complexes can display a stronger emission intensity and a longer lifetime relative to the cellular backgrounds, making them clearly distinguishable on the collected intensity and lifetime images. These emission signals were also identified as round spots close to those from the single metal nanoprobes (Fig. 1), indicating that the metal nanoprobes were mostly presented as either individuals or small aggregates on the tissues.

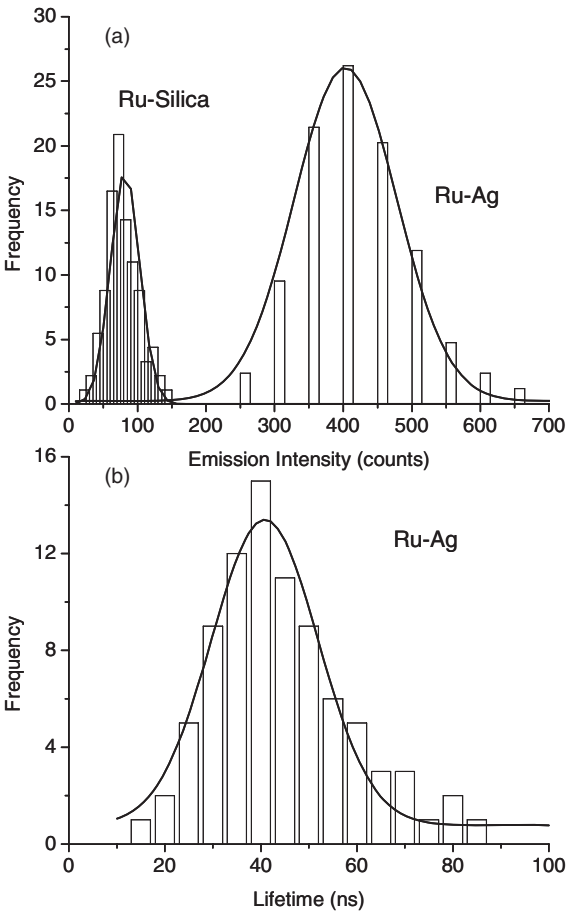

Fig. 2 Distributions of (a) emission intensity and (b) lifetime for the silica spheres and silver nanoshells. Because of instrument limitation, the lifetime of single silica spheres cannot be determined accurately on the current confocal microscope. This lifetime has previously been measured using ensemble time-resolved spectroscopy (Ref. 13).

To identify the locations of the metal nanoprobes, the tissue specimens were stained with 1,2-dihexadecanoyl-sn-glycero-3-phosphoethanolamine triethylammonium salt on the cell membranes and YOYO-1 iodide on the cell nucleus.[20] In comparison with the nonstained tissues, the stained specimens expressed significantly increased cellular backgrounds due to additional dyes [Figs. 3(c) and 4]. As a result, some emission signals from the avidin-FMN complexes became unidentifiable on the intensity images [Fig. 3(c)]. On the other hand, these additional staining dyes have their lifetimes close to the lifetime of cellular autofluorescence but shorter than the lifetime of metal nanoprobes. Therefore, the emission signals of metal nanoprobes could be absolutely isolatable on the lifetime images [Fig. 3(d)].

To further interpret these observations, the intensity and lifetime data throughout the images were analyzed by Gaussian

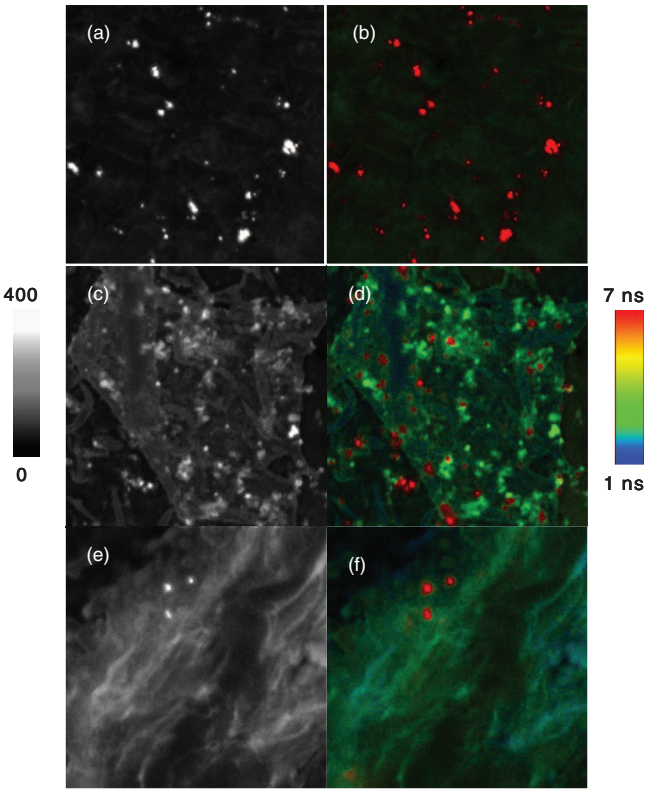

Fig. 3 Representative images of tissue specimens prior to staining in (a) intensity and (b) lifetime and those after staining in (c) intensity and lifetime (d) images. The tissue specimens were stained with 1,2-dihexadecanoyl-sn-glycero-3-phosphoethanolamine triethyl ammonium salt on the cell membranes and YOYO-1 iodide on the nucleus. The scales of images are 50×50 μm and the resolutions are 500×500 pixel with an integration of 0.6 ms/pixel. The tissues without biotinylation treatments were also incubated with the avidin-FMN complexes and the images in (e) intensity and (f) lifetime were collected as controls.

distributions and the distribution curves are given in Fig. 4. It was shown that the distribution curve of intensity over the cellular background was almost entirely separated with the curve of the conjugated avidin-FMN complexes [Fig. 4(a)]. It was the reason that the emission signals from the avidin-FMN complexes could be distinctly isolated from the cellular backgrounds on the intensity images prior to staining. However, with the staining by additional dyes, the cellular backgrounds in the intensity images significantly increased, leading to the distribution curve of cellular background shifting higher and overlapping with the distribution curve of avidin-FMN complexes. Consequently, some emission signals from the avidin-FMN complexes could not be distinctly identified. On the other hand, the distribution curve of cellular background over the lifetime image was almost regardless of the presence of additional dyes by staining and has a maximum of 3 ns [Figs. 4(b) and 4(c)]. Even though the distribution curve of avidin-FMN complexes on the lifetime images was shifted shorter with the staining due to interferences from additional dyes, there was not a overlapping with the curve of cellular background. As a result, even when the tissues were stained, the emissions from the metal nanoprobes could be isolated clearly from the cellular backgrounds on the lifetime images.

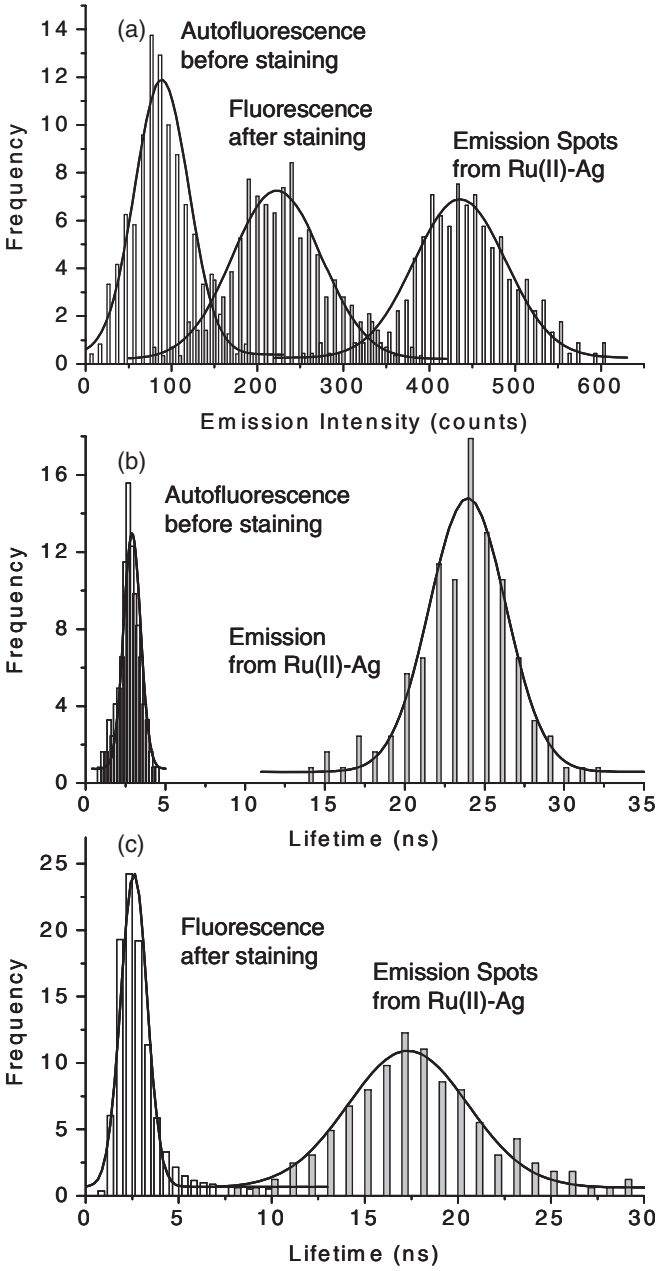

Fig. 4 (a) Represents intensity distributions by the cellular autofluorescence throughout the intensity image of blank tissue, by the stained dyes on the image of stained tissue, and by the avidin-FMN complexes on the intensity image. (b) Represents the lifetime distributions by the cellular autofluorescence throughout the image of blank tissue and the avidin-FMN complexes on the lifetime image. (c) Represents the lifetime distributions throughout the image of stained tissue and the avidin-FMN complexes on the lifetime image.

We also noticed that the emission signals from the avidin-FMN complexes could be counted on the single cell images [Fig. 3(c)]. To better isolate the signals of metal nanoprobes from the cellular backgrounds, we analyzed the lifetime images with OriginPro-7 software. First, lifetime data with the values greater than 10 ns were removed because they were regarded from cellular autofluorescence. The residual data were converted to an image. It was observed that the cellular backgrounds on this image became dim and almost disappeared. As

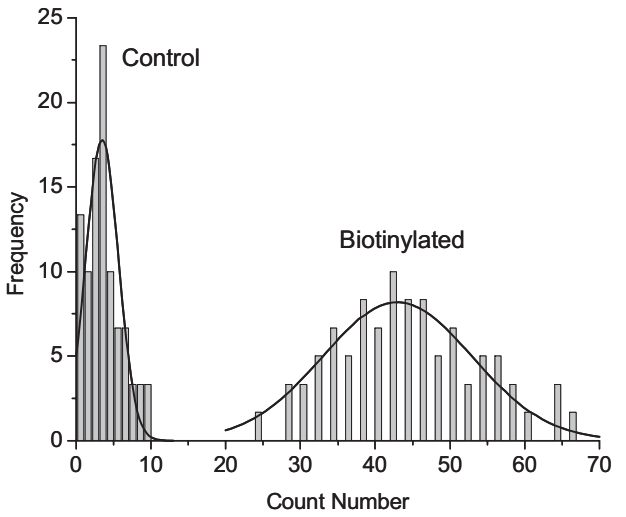

Fig. 5 Distribution of the count numbers by the avidin-FMN complexes appearing on 50×50 μm image from the biotinylated tissues. Distribution on the treated tissues was also collected under the same conditions as control.

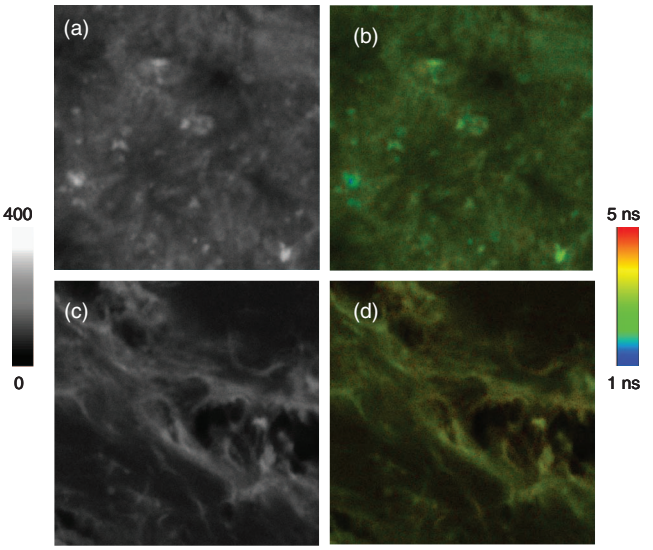

Fig. 6 Representative (a) intensity and (b) lifetime images of tissue specimens with the Rhodamine 6G avidin conjugates. The scales of images are 50×50 μm and the resolutions are 500×500 pixel with an integration of 0.6 ms/pixel. Representative (c) intensity and (d) lifetime images of tissues without biotinylation treatments were also collected under the same conditions as controls.

a result, the emission spots from the metal nanoprobes were identified uniformly and counted precisely. At least 20 images of 50×50 μm scales were analyzed. The statistical results are listed in Fig. 5. An average of 45 emission spots per image was obtained. This number may not reflect the actual number of metal nanoprobes on the image areas. The reason is that one emission spot may represent the emission signals from several metal nanoprobes that cannot be resolved due to low resolution of the microscope. Nevertheless, this result may provide a semi-quantitative approach for direct observation to the amounts and distributions of target molecules on the tissue specimens. Most tissue images are currently validated by the changes of emission intensity over the entire images and the emission signals from the probes cannot be completely resolved from the cellular backgrounds. The approach developed in this research is thus regarded as a significant advance for clinical applications.

To examine the affinity of metal nanoprobes, we also incubated the tissue specimens without biotinylation treatment with the avidin-FMN complexes. These tissue images were collected under the same conditions. It was observed that there were much fewer emission spots on the intensity and lifetime images with the same areas [Figs. 3(e) and 3(f)]. In the same treatments, the count number is only 5 (Fig. 5), less than the number on the biotinylated tissues, implying that the avidin-FMN complexes can be site-specially conjugated with the tissue specimens. We also notice that there is no significant aggregate of nanoparticle probe on the cell images, which is contrary to the result on the biotinylated tissue images (Fig. 2), indicating that the aggregates were caused by high concentration of biotin sites on the tissue specimens.

To confirm the importance of metal nanoprobes in imaging, we also incubated the biotinylated tissues with Rhodamine 6G-avidin conjugates [Figs. 6(a) and 6(b)]. The tissue specimens without biotinylation treatment were also incubated with Rhodamine 6G-avidin conjugates [Figs. 6(c) and 6(d)]. Compared with the images of tissues without biolytination treatment, the images of biotinylated tissues displayed a significant increase on the overall emission intensity, indicating that the avidin conjugates were bound on the tissues. However, their emission signals could not be isolated individually on both the intensity or lifetime images. It is worth noticing that these tissues were not stained by additional organic dyes. Once the tissues were stained, it becomes more difficult to isolate the emission signals of metal-free conjugates from the cellular backgrounds.

4 Conclusion

We report a fluorescence imaging approach for target molecule detection on bone tissue specimens using FMNs. Since the metal nanoprobes displayed increased emission intensity and a unique lifetime, the emission signals from the single nanoprobes could be distinctly isolated from cellular backgrounds in the intensity and lifetime images. A lifetime imaging method is regarded to be better when the tissues were stained with additional organic dyes.

Acknowledgments

This research was supported by grants from NIH (EB009509, HG-002655, HG005090, EB006521, and CA147975).

References

1. H. Kobayashi, M. Ogawa, R. Alford, P. L. Choyke, and Y. Urano, "New strategies for fluorescent probe design in medical diagnostic imaging," *Chem. Rev.* **110**, 2620–2640 (2010).
2. J. R. Lakowicz, *Principles of Fluorescence Spectroscopy*, 3rd Ed., Kluwer Academic/Plenum Publishers, New York (2006).
3. K. Licha, B. Riefke, V. Ntziachristos, A. Becker, B. Chance, and W. Semmler, "Breast imaging technology: Probing physiology and molecular function using optical imaging - applications to breast cancer," *Photochem. Photobiol.* **72**, 392–398 (2000).

4. A. Mishra, R. K. Behera, P. K. Behera, B. K. Mishra, and G. B. Behera, "Cyanines during the 1990s: a review," *Chem. Rev.* **100**, 1973–2012 (2000).
5. M. Y. Berezin and S. Achilefu, "Fluorescence lifetime measurements and biological imaging," *Chem. Rev.* **110**, 2641–2684 (2010).
6. S. Lee, J. Xie, and X. Chen, "Peptides and peptide hormones for molecular imaging and disease diagnosis," *Chem. Rev.* **110**, 3087–3111 (2010).
7. P. K. Jain, X. Huang, I. H. El-Sayed, and M. A. El-Sayed, "Noble metals on the nanoscale: optical and photothermal properties and some applications in imaging, sensing, biology, and medicine," *Acc. Chem. Res.* **41**, 1578–1586 (2008).
8. R. Bardhan, N. K. Grady, J. R. Cole, A. Joshi, and N. J. Halas, "Fluorescence enhancement by Au nanostructures: nanoshells and nanorods," *ACS Nano* **3**, 744–752 (2009).
9. J. R. Lakowicz, "Radiative decay engineering 5: metal-enhanced fluorescence and plasmon emission," *Anal. Biochem.* **337**, 171–194 (2005).
10. M. A. van Dijk, M. Lippitz, and M. Orrit, "Far-field optical microscopy of single metal nanoparticles," *Acc. Chem. Res.* **38**, 594–601 (2005).
11. Y. Fu, J. Zhang, and J. R. Lakowicz, "Silver-enhanced fluorescence emission of single quantum dot nanocomposites," *Langmuir* **24**, 3429–3433 (2008).
12. J. Zhang, Y. Fu, M. H. Chowdry, and J. R. Lakowicz, "Plasmon-coupled fluorescence probes: effect of emission wavelength on fluorophore-labeled silver particles," *J. Phys. Chem. C* **112**, 9172–9180 (2008).
13. J. Zhang, Y. Fu, and J. R. Lakowicz, "Emission behavior of fluorescently labeled silver nanoshell: enhanced self-quenching by metal nanostructure," *J. Phys. Chem. C* **111**, 1955–1961 (2007).
14. J. Zhang, Y. Fu, and J. R. Lakowicz, "Luminescent silica core/silver shell encapsulated with Eu(III) complex," *J. Phys. Chem. C* **113**, 19404–19410 (2009).
15. J. Zhang, Y. Fu, D. Liang, K. Nowaczyk, R. Y. Zhao, and J. R. Lakowicz, "Single-cell fluorescence imaging using metal plasmon-coupled probe 2: single-molecule counting on lifetime image," *Nano Lett.* **8**, 1179–1186 (2008).
16. J. Zhang, Y. Fu, D. Liang, K. Nowaczyk, R. Y. Zhao, and J. R. Lakowicz, "Fluorescent avidin-bound silver particle: a strategy for single target molecule detection on a cell membrane," *Anal. Chem.* **81**, 883–889 (2009).
17. R. Bardhan, N. K. Grady, T. Ali, and N. J. Halas, "Metallic nanoshells with semiconductor cores: optical characteristics modified by core medium properties," *ACS Nano* **4**, 6169–6179 (2010).
18. S. Lal, S. E. Clare, and N. J. Halas, "Nanoshell-enabled photothermal cancer therapy: impending clinical impact," *Acc. Chem. Res.* **41**, 1842–1851 (2008).
19. J. Zhang, Y. Fu, Y. Mei, F. Jiang, and J. R. Lakowicz, "Fluorescent metal nanoshell probe to detect single miRNA in lung cancer cell," *Anal. Chem.* **82**, 4464–4471 (2010).
20. J. Zhang, Y. Fu, G. Li, R. Y. Zhao, and J. R. Lakowicz, "Detection of CXCR4 receptors on cell surface using a fluorescent metal nanoshell," *J. Biomed. Opt.* **16**, 016011 (2011).
21. M. Monici, "Cell and tissue autofluorescence research and diagnostic applications," *Biotechnol. Annu. Rev.* **11**, 227–256 (2005).
22. I. H. El-Sayed, X. Huang, F. Macheret, R. Kramer, and M. El-Sayed, "Effect of plasmonic gold nanoparticles on benign and malignant cellular autofluorescence: a novel probe for fluorescence based detection of cancer," *Technol. Cancer Res. Treat.* **6**, 403–412 (2007).
23. J. Zhang, D. Roll, C. D. Geddes, and J. R. Lakowicz, "Aggregation of silver nanoparticle-dextran adducts with concanavalin A and competitive complexation with glucose," *J. Phys. Chem. B* **108**, 12210–12214 (2004).
24. A. C. Templeton, W. P. Wuelfing, and R. W. Murray, "Monolayer-protected cluster molecules," *Acc. Chem. Res.* **33**, 27–36 (2000).
25. M. Brinkley, "A brief survey of methods for preparing protein conjugates with dyes, haptens and crosslinking reagents," *Bioconjugate Chem.* **3**, 2–13 (1992).
26. C. Wersinger, P. Vernier, and A. Sidhu, "Trypsin disrupts the trafficking of the human dopamine transporter by alpha-synuclein and its A30P mutant," *Biochemistry* **43**, 1242–1253 (2004).
27. C. Wersinger and A. Sidhu, "Disruption of the interaction of alpha-synuclein with microtubules enhances cell surface recruitment of the dopamine transporter," *Biochemistry* **44**, 13612–13624 (2005).
28. N. L. Rosi and C. A. Mirkin, "Nanostructures in biodiagnostics," *Chem. Rev.* **105**, 1547–1562 (2005).